Available online at www.sciencedirect.com
ScienceDirect
Journal of Sound and Vibration 323 (2009) 697–717
JOURNAL OF SOUND AND VIBRATION
www.elsevier.com/locate/jsvi

An equivalent-source model for simulating noise generation in turbofan engines

C. Polacsek*, G. Desquesnes, G. Reboul

Numerical Simulations and Aeroacoustics Department, ONERA, BP 72, 92322 Châtillon Cedex, France

Received 26 October 2007; received in revised form 6 January 2009; accepted 9 January 2009
Handling Editor: P. Joseph
Available online 27 February 2009

Abstract

Nowadays, computational aeroacoustics (CAA) is used for simulating wave propagation in ducted turbofans, especially as computational fluid dynamics (CFD) is increasingly employed to model the identified noise sources. An efficient way to match the CFD and CAA domains is to make some assumptions on flow and duct geometry, so that disturbance fields can be expanded over incoming/outgoing acoustic modes. Based on this approach, this paper presents an original matching model in which the outgoing modes are generated by means of equivalent monopole distributions defined as source terms in the equations governing the acoustic propagation, instead of a conventional inflow boundary condition (BC). Advantages and limits of the method are discussed. The process to get back to the sources and its numerical implementing are described. Although initially focused on tones, an extension of the method to broadband noise generation is tackled too. The method then is validated on a simplified turbofan exhaust configuration. Numerical solutions obtained by implementing the source terms in a high-order time-domain Euler code are compared to analytical solutions, either in a uniform or in a radially shear mean flow (provided by RANS). The parallel shear flow solution is obtained by solving the Pridmore–Brown equation. The ability to accurately simulate the standing waves due to acoustic reflections at duct ends is also assessed by comparing the numerical solutions computed using both source-based and BC-based options in the Euler solver.

1. Introduction

Fan noise generated by rotor–stator interaction mechanisms is one of the major contributions to tone spectrum level of high-bypass ratio aeroengines during take-off and approach [1]. A great attention is paid now to reduce these tones highly dominating the overall sound pressure levels, especially as air traffic is growing and environmental rules become drastic regarding with ACARE (Advisory Council for Aeronautical Research in Europe) objectives.

In the aim of reducing noise, accurate models and numerical tools are needed for simulating noise generation and acoustic in-duct propagation including both realistic geometry and convection effects. Such advanced tools are very helpful for the design and analysis of novel technologies. Hybrid methods consisting

*Corresponding author.
E-mail address: cyril.polacsek@onera.fr (C. Polacsek).

0022-460X/$ - see front matter © 2009 Elsevier Ltd. All rights reserved.
doi:10.1016/j.jsv.2009.01.010

in splitting the fan noise problem into a source problem and a propagation problem, respectively, using computational fluid dynamics (CFD; RANS solvers) and computational aeroacoustics (CAA; Euler or potential flow solvers) are commonly adopted today [2–5]. In this approach, sketched in Fig. 1, a crucial issue concerns the "coupling" between the two computation domains that is generally achieved by means of a matching procedure [6]. In this study we adopt a wave-splitting technique, initially proposed by Rienstra [7] in the framework of European project TurboNoiseCFD. It is based on the expansion of a local perturbation field (along the matching plane) into outgoing/incoming modes, and on a propagation model satisfying local assumptions for flow and geometry.

The modal approach is briefly presented in Section 2.1. This first step is conventional, and the original part of the method (second step detailed in Section 2.2) is that the outgoing modes are generated in terms of equivalent monopoles to be entered as source inputs in the CAA, rather than boundary conditions (BC) [8]. This key point is sketched in Fig. 2, relative to a bypass duct. The "matched solution" defined at the CFD/CAA interface should ideally satisfy two primary non-trivial conditions (involving continuity of acoustic perturbations across the matching plane):

(1) To simulate an outgoing wave, P_{out}, provided by the wave-splitting procedure.
(2) To converge to a total acoustic field equal to the sum of the outgoing wave and of the reflected wave, P_{reflect}, due to impedance discontinuity at outlet duct end (or in the presence of a liner).

A typical difficult problem concerned with the two conditions is the propagation of an acoustic mode inside a nacelle with liner splices, requiring solution of a complex matrix system at each discontinuity [9]. Suitable formulations can be derived in the frequency domain, by splitting the vector-solution into outgoing (inputs) and reflected (unknowns) modes, as is done in Ref. [10] for nacelle propagation studies. For the Euler problem in the time domain, some authors [4,11] use a suitable BC in order to enforce the numerical solution to a target (P_{out}), by applying a damping buffer zone in the upstream region (in grey in Fig. 2). The difficulty then is to find a practical way to prevent from artificial reflections due to the pressure jump at the interface, since the

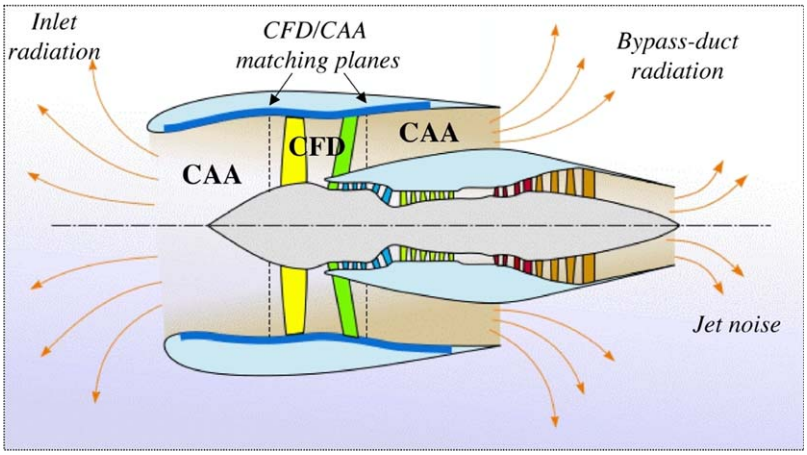

Fig. 1. Sketch of turbofan aeroacoustic problem (from Ref. [7]).

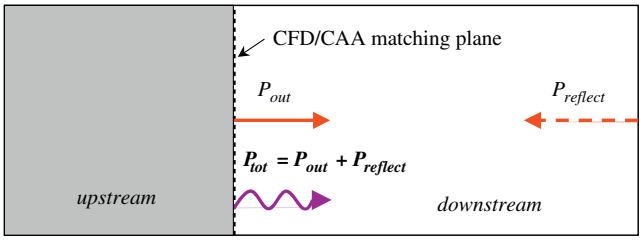

Fig. 2. Sketch of the matching problem (bypass duct case).

incoming disturbances (reflected waves from open duct end) in the buffer zone are set to zero at each time step. A numerical implementing of a so-called "injection condition" in the ONERA CAA code *sAbrinA* [12,13] will be briefly described. Anyway, ability of these approaches to simulate accurate propagation in the presence of standing waves is not obvious and should be still more investigated.

Another way is suggested here to avoid this difficulty is by fitting the target by means of equivalent sources located on the matching plane, so that the total field is no longer imposed and remains free. Non-reflecting boundary conditions (NRBC) in the upstream direction are simply ensured by adding a few stretched cells behind the matching plane (acting as a damping zone here too). Numerical implementation of this equivalent source term, detailed in the present paper, might be easier than the BC approach requiring management of fictive cells where the initial conditions must satisfy the causality law [12]. Hence, the suggested coupling method appears well suited to many turbofan noise applications such as nacelle geometry design, or liner optimization inside the nacelle, since the standing waves are significant at low-frequency and must be accurately captured.

Following sections of the paper are devoted to the description of the equivalent-source model and to its numerical implementation in *sAbrinA*. The model (initially developed for tones) is extended to broadband noise generation. An overview of the computation of the equivalent sources using a Matlab code called *ExFan* (Equivalent Source Fan), and a short description of CAA code *sAbrinA* are proposed. The numerical implementation of these sources as an equivalent source term in *sAbrinA* is detailed. Then, third section is devoted to selected benchmarks and their validations, highlighted by some comparisons between BC-based and source-based numerical simulations issued from *sAbrinA*. To conclude, a few perspectives of the methodology are discussed.

2. Equivalent-source model

2.1. Modal approach

The propagation model locally considered at the CFD/CAA interface assumes a uniform mean flow with isentropic perturbations in a straight annular duct with rigid walls. Rienstra developed a general formulation based on a multiple-scale method [14], taking into account a slowly varying duct section and an isentropic potential flow, but the present work is limited to a more conventional approach, in order to easily get back to the sources. Realistic geometry and convection effects are supposed to be taken into account when coupling with CAA. In these conditions, the harmonic pressure disturbance field on angular frequency ($\omega = 2\pi f$) can be expanded over Fourier–Bessel spinning modes, with circumferential order m and radial order μ:

$$p(z,r,\theta,t) = \sum_{m,\mu} p^{\pm}_{m\mu} C_{m\mu}\left(\alpha_{m\mu}\frac{r}{R}\right) \mathrm{e}^{\mathrm{i}(\omega t - m\theta - k^{\pm}_{m\mu} z)} \tag{1}$$

The $C_{m\mu}$ are a combination of Bessel functions with a normalization factor proposed by Rienstra (see Ref. [5] for a full description), with associated eigenvalues, $\alpha_{m\mu}$. $p_{m\mu}$ are the complex modal amplitudes, $k_{m\mu}$ is the axial wave number, and $\pm$ denotes outgoing ($+$) or incoming ($-$) waves. Eq. (1) is currently adopted in the inlet region (Fig. 1) where the flow is almost potential, but it can also be applied in the bypass region (Figs. 1 and 2) in the presence of an axial shear flow without vortical waves (assumed to be negligible), as it will be shown later. Note that assumptions (uniform mean flow and constant duct section) have to be valid only in the matching region, beyond which smooth geometry variation and convection effects are expected to be taken into account by the propagation solver. Moreover, turning-point phenomenon [14] that might arise for nearly cut-off modes is also simulated here by including the first cut-off modes in Eq. (1), as discussed below.

2.2. Equivalent sources

The Green's function, G, in cylindrical coordinates (in a fixed reference frame linked to the duct) is expressed in a uniform mean flow:

$$G(\vec{X}_s|\vec{X},t) = \sum_{m,\mu} \frac{i}{4\pi R^2 \Delta_{m\mu}} C_{m\mu}\left(\alpha_{m\mu}\frac{r_s}{R}\right) C_{m\mu}\left(\alpha_{m\mu}\frac{r}{R}\right) \exp\{\mathrm{i}(\omega t - m(\varphi-\varphi_s) - k^{\pm}_{m\mu}(z-z_s))\} \tag{2}$$

In Eq. (2), $\Delta_{m\mu}$ is the determinant deduced from the classical dispersion relation, and source ($\vec{X}_s$) and observer ($\vec{X}$) locations are defined as

$$\vec{X}_s = \{r_s, \varphi_s, z_s\}, \quad \vec{X} = \{r, \varphi, z\}$$

The modal Green's function, $G_{m\mu}$, that refers only to the radial position of the source, r_s, writes:

$$G_{m\mu}(r_s) = \frac{i}{4\pi R^2 \Delta_{m\mu}} C_{m\mu}\left(\alpha_{m\mu}\frac{r_s}{R}\right) \tag{3}$$

Starting from the knowledge of the modal amplitudes, $p_{m\mu}$, practically deduced from the CFD disturbance field by means of a standard [5,6] or more advanced [7] wave-splitting technique, the radial pressure profile related to the angular mode m, $p_m(r)$, can be generated using a point-source distribution along the radius, following Eqs. (4a) and (4b):

$$p_m(r) = \sum_{\mu=1}^{\mu_{\max}} p_{m\mu} C_{m\mu}\left(\alpha_{m\mu}\frac{r}{R}\right) \tag{4a}$$

$$p_{m\mu} = \sum_{j=1}^{j_{\max}} q^j A_{m\mu}(r_s^j) \tag{4b}$$

$A_{m\mu}$ represents an elementary modal amplitude, solution of the semi-infinite annular duct with uniform mean flow problem, in the presence of a monopole source q^j at radial position r_s^j. It is related to the modal Green's function $G_{m\mu}$ as [5]

$$A_{m\mu}(r_s)\exp\{\mathrm{i}(\omega t - k_{m\mu}^{\pm} z)\} = \frac{\mathrm{d}}{\mathrm{d}t}[G_{m\mu}(r_s)\exp\{\mathrm{i}(\omega t - k_{m\mu}^{\pm} z)\}] \tag{5a}$$

$$A_{m\mu}(r_s) = \mathrm{i}(\omega \pm c_0 M k_{m\mu}^{\pm}) G_{m\mu}(r_s) \tag{5b}$$

where M is the mean flow Mach number and c_0 is the speed of sound. $\mathrm{d}/\mathrm{d}t$ is the convective derivation operator:

$$\frac{\mathrm{d}}{\mathrm{d}t} = \frac{\partial}{\partial t} \pm c_0 M \frac{\partial}{\partial z}$$

where $\pm$ denotes downstream ($+$) or upstream ($-$) case.

In this way, amplitude of each monopole, q^j, relative to a single mode m, is obtained by solving the following matrix system:

$$[A_{m\mu}(r_s^j)][q^j] = [p_{m\mu}] \tag{6}$$

A solution only exists under the condition $j_{\max} \geqslant \mu_{\max}$, where $\mu_{\max}$ is the maximum order of radial modes considered. Note that there is no restriction about evanescent modes (k complex) that can be also included in the model. Practically, we set $j_{\max} = \mu_{\max}$, and we include first cut-off modes in order to increase stability and accuracy in the numerical process, and to take into account possible turning-point effect, as mentioned in the previous section. Selected spinning mode order, m, is generated using a continuous source-ring angular distribution, which will be described in Section 2.4. Equivalent sources are computed using Matlab routines packed in the code *ExFan*.

2.3. Description of sAbrinA code

ONERA has been working for several years on the design of a multi-purpose integrated CFD/CAA solver based on the discretization of the compressible Navier–Stokes equations on multi-block structured meshes by use of a cell-centered finite volume technique. Recently, specific acoustic features (finite difference, high order schemes, splitted variables) have been implemented in this platform, renamed *sAbrinA*. More details can be found in Refs. [12,13]. For engine noise problems, the code is particularly able to solve the full Euler equations

applied to the disturbances, aiming at simulating nonlinear acoustic propagation in complex flows (as for jet noise, or exhaust propagation through realistic shear flows). The main features of the CAA solver are the following:

- Euler equations, in complete or splitted variables.
- High order finite difference curvilinear schemes (up to sixth order).
- High order filtering schemes (up to 14th order).
- Explicit (third order) temporal scheme.
- Specific inflow BC and source-terms (including acoustic modes).

Generalized multidimensional NRBC are still required in *sAbrinA*, featuring only conventional Thomson conditions, known to be unsuited in the case of 3D acoustic waves. For this reason, a simple but efficient grid stretching technique is employed here to simulate free-space conditions. Non-dispersive and non-dissipative acoustic propagation is ensured using $\lambda/10$ grid spacing in the axial direction (λ denoting the smallest axial wavelength). The time spacing is adjusted so that the CFL (Courant–Friedrich–Lewy) number is almost equal to 1, in order to limit the number of time iterations required for getting a periodical solution.

Acoustic modes can be directly generated using an inflow BC (''injection'' condition), initially developed by Redonnet. The implementation is done by the use of fictive cells (5 for the selected numerical schemes). It consists in imposing a downstream analytical solution given by Eq. (1) in the fictive cells at each time step, and taking into account the phase dependency. As discussed in the introduction, such an approach assumes that incoming waves can be neglected.

Alternatively, these modes can be also ''injected'' by means of equivalent sources. This is the scope of the present paper, and the numerical implementation in *sAbrinA* is described in following section.

2.4. Numerical implementation of the equivalent source-term in sAbrinA

The Euler disturbance equations with source terms are written in a linearized non-conservative form, given by Eq. (7a). Under the assumptions discussed in Section 2.1, they lead to the non-homogeneous convected wave equation given by Eq. (7b):

$$\begin{cases} \dfrac{\mathrm{d}\rho}{\mathrm{d}t} + \rho_0 \vec{\nabla}\cdot\vec{u} = s_\rho \\ \rho_0 \dfrac{\mathrm{d}\vec{u}}{\mathrm{d}t} + \vec{\nabla} p = s_u \\ \dfrac{\mathrm{d}p}{\mathrm{d}t} + \gamma p_0 \vec{\nabla}\cdot\vec{u} = s_p \end{cases} \tag{7a}$$

$$\Delta p - \frac{1}{c_0^2}\frac{\mathrm{d}^2 p}{\mathrm{d}t^2} = -\frac{\mathrm{d}s_\rho}{\mathrm{d}t} \tag{7b}$$

In these equations ρ, p, u are the density, the pressure, and the velocity disturbances, respectively, and s relates to the source term. Eq. (7b) is deduced from Eq. (7a) by assuming an isentropic acoustic pressure mode generated by harmonic point-source, q, located at $\vec{X}_s^0$, and defined as

$$\begin{cases} s_p = s_\rho c_0^2 \\ s_u = 0 \\ c_0^2 = \dfrac{\gamma p_0}{\rho_0} \end{cases}, \quad s_\rho(\vec{X}_s, t) = q(\vec{X}_s^0)\delta(\vec{X}_s - \vec{X}_s^0)\sin(\omega t) \tag{8}$$

Note that such a description of isentropic modes assumes that acoustic, vortical and entropic disturbances are fully decoupled. More advanced models proposed by Peake [15] or Atassi [16] aiming at solving the complicated matching problem in swirling flows are out of the scope of our study. So, it is expected that no

entropic neither vortical modes are excited in the source-region. It is the same when the modes are imposed in terms of the inflow BC previously described.

The Dirac function in Eq. (8) can be approached by a suitable normalized Gaussian-distribution generalized here to n-dimensional problems:

$$\delta(\vec{X}_s - \vec{X}_s^0) \approx \frac{1}{b^n} \mathrm{e}^{-\pi((\vec{X}_s - \vec{X}_s^0)^2/b^2)} \tag{9}$$

Hence, a spinning acoustic mode of order m is numerically implemented in *sAbrinA* using a pulsating source ring, s_ρ^m, that can be expressed as

$$\begin{cases} s_\rho^m(\vec{X}_s, t) = \sum_{j=1}^{j_{\max}} \dfrac{|q^j(r_s^j)|}{2\pi r_s^j b^2} \mathrm{e}^{-\pi(\hat{r}^2/b^2)} \sin(\omega t - m\varphi_s + \phi^j) \\ \hat{r} = ((r_s - r_s^j)^2 + (z_s - z_s^0)^2)^{1/2}, \quad r_s = (x_s^2 + y_s^2)^{1/2}, \quad \varphi_s = \tan^{-1}\left(\dfrac{y_s}{x_s}\right) \end{cases} \tag{10}$$

In Eq. (10), x, y, z (r, φ, z in cylindrical) denote the Cartesian coordinates, and subscript s relates to the source. z_s^0 is the axial position of the source plane, and φ_s^j (angular position of reference for all sources) is set equal to zero. Complex values of equivalent monopoles q^j, with amplitude $|q^j|$ and phase ϕ^j, are obtained from Eq. (6). b defines the width of the Gaussian pulse that is adjusted to fit the norm (Δr) of the neighboring cells. Indeed, parametric studies made on non-dimensioned regular grids ($\Delta x = \Delta y = \Delta z = 1$) have shown that this Gaussian distribution was stable and accurate (independent of the acoustic wave number) if $1 \leqslant b \leqslant 3$, and optimal for $b = \Delta r = (\Delta x^2 + \Delta y^2 + \Delta z^2)^{1/2} = \sqrt{3}$. Sketches of equivalent sources are presented in Fig. 3a and b, showing, respectively, a sampled distribution (discrete monopoles) and a continuous distribution (rings as in Eq. (10)), in the case $\mu_{\max} = 1$. The number of rings to be used is equal to $\mu_{\max}$.

The 1D Gaussian distributions $(1/b)\,\mathrm{e}^{-\pi(\hat{r}^2/b^2)}$ (with area equal to unity), and a representation of parameter b over a regular cartesian grid, are shown, respectively, in Fig. 4a and b. A typical result comparing analytical solution and numerical computation (with $b = 1$, 2, and 3) of a harmonic Green's function (plane mode case) solution of Eq. (2) is presented in Fig. 5, showing that best accuracy is achieved for $b = \Delta r \approx 2$.

Note that the method permits to generate selected single modes (useful for parametrical studies or benchmarks as here) and also, for practical applications, to generate overall propagating modes on all interaction tones, as done recently in Ref. [17].

2.5. Extension to broadband noise generation

Although initially developed for tone noise studies, this equivalent-source model can be extended to broadband noise applications, using turbulent data information provided for instance by an LES (large Eddy

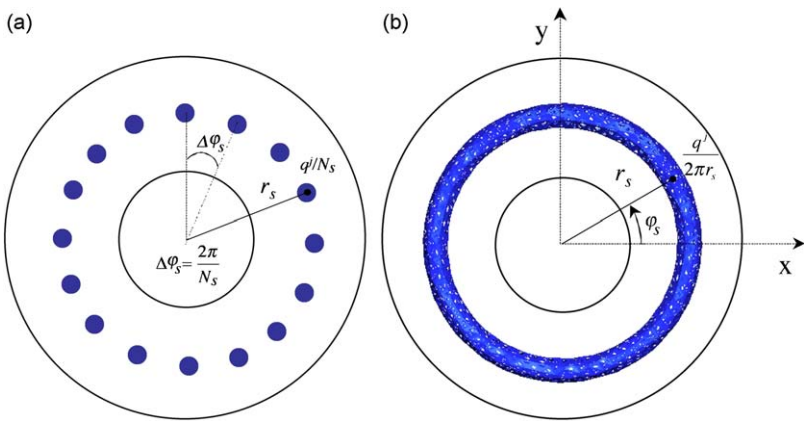

Fig. 3. Generation of spinning modes using discrete (a) or continuous (b) source-ring distribution.

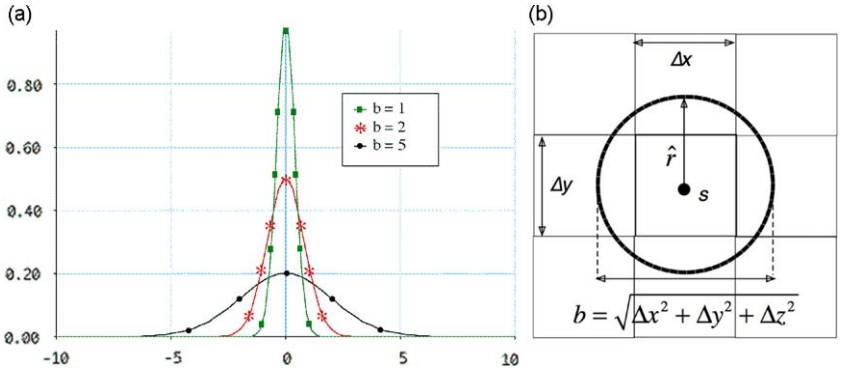

Fig. 4. Numerical implementing of a Dirac function in *sAbrinA* code: (a) Gaussian distributions; (b) pulse width adjustment.

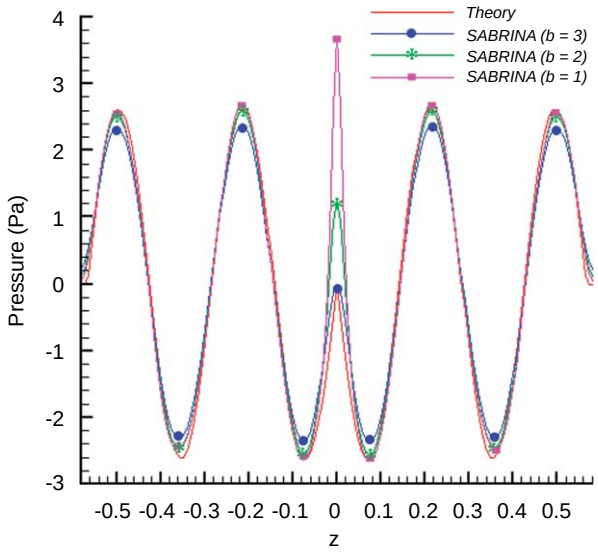

Fig. 5. Comparison between analytical and numerical harmonic Green's function for a plane wave in a semi-infinite annular duct.

simulation) computation [18]. A short description is proposed here, and a basic validation will be presented in Section 3.3. The idea is still to use suitable harmonic sources with random phases, able to generate a turbulent-like acoustic field providing a multi-mode and multi-frequency sampling of the power spectrum density (PSD). A typical frequency-mode distribution in an annular duct is shown in Fig. 6. A generic PSD, $S(f)$, with equivalent sampled spectrum, $\tilde{S}(f_i)$, are sketched in Fig. 7a and b. The prescribed PSD of Fig. 7a, expected to be known in the matching plane (the way to get it is out of scope here), is assumed to verify the usual non-coherent mode assumption currently used in ducted-fan broadband noise applications:

$$S(f,r) = \sum_{m,\mu} S_{m\mu}(f,r) \tag{11a}$$

$$S_{m\mu}(f,r) = |P_{m\mu}(f)C_{m\mu}(r)|^2 = W_{m\mu}(f)C^2_{m\mu}(r) \tag{11b}$$

By this way, the same matching process that is done for the tones can be used. Sampled complex modal harmonics, $\tilde{P}^k_{m\mu}(f_i)$, at selected frequency, f_i, and for a single realization (index k), can be expressed from

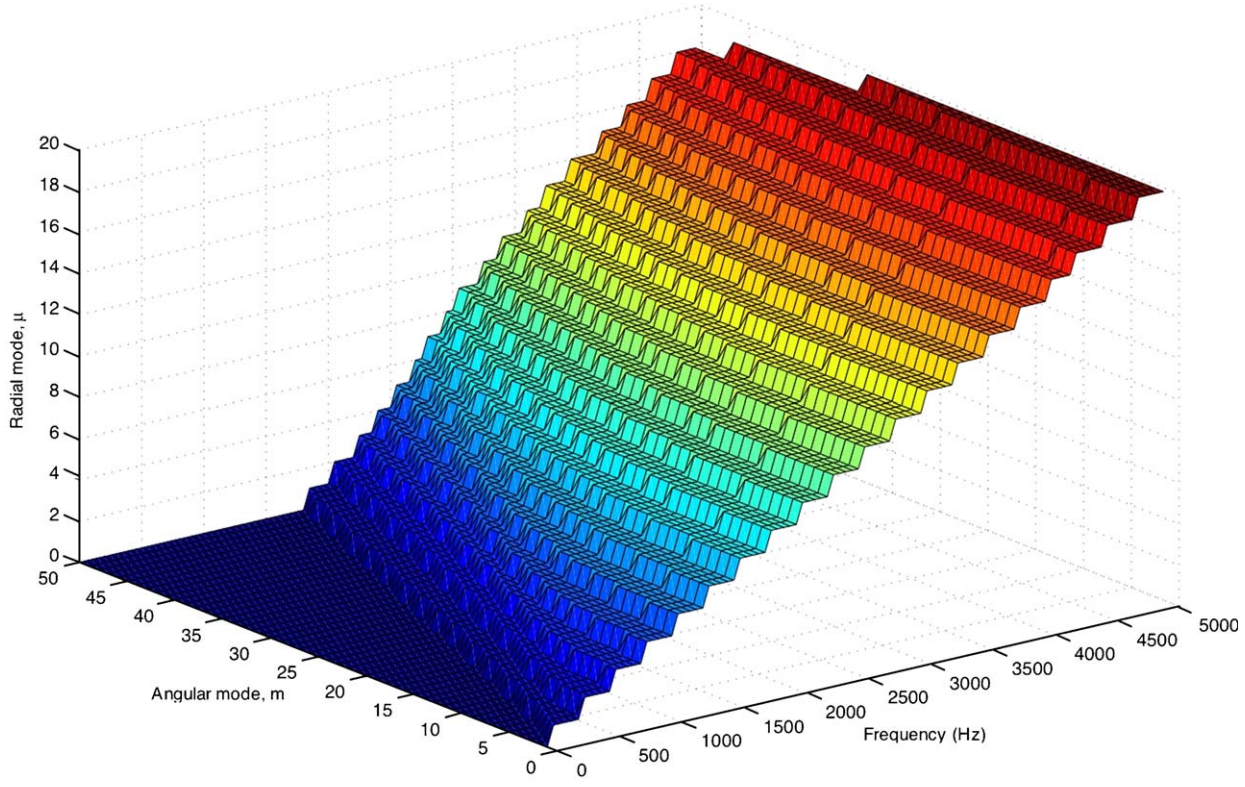

Fig. 6. Frequency-mode distribution in an annular duct (outer radius $R = 1.46\,\mathrm{m}$, hub-to-tip ratio $h = 0.57$).

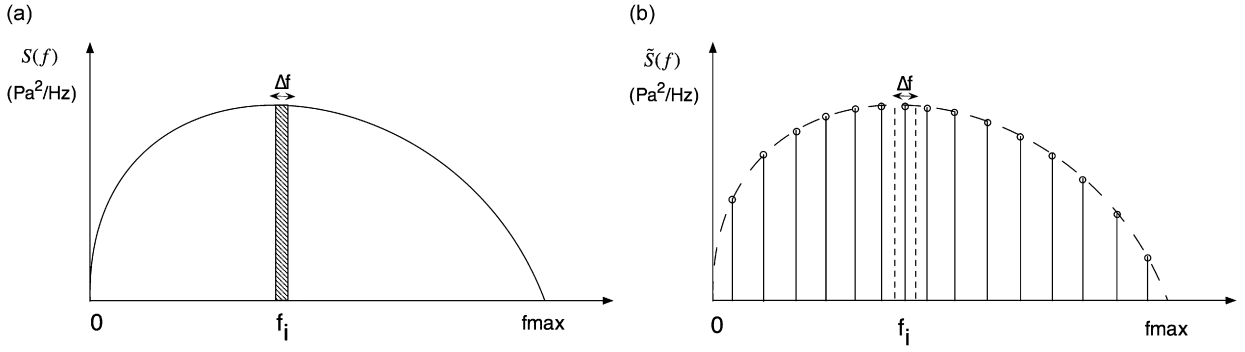

Fig. 7. Continuous PSD generated by turbulent sources (a) and sampled PSD generated by equivalent harmonic sources (b).

Eq. (4b) as :

$$\tilde{P}^k_{m\mu}(f_i) = |\tilde{P}_{m\mu}(f_i)|\mathrm{e}^{\mathrm{i}\phi^k_{m\mu}} = \left\{\sum_{j=1}^{j_{\max}} q^{jk} A_{m\mu}(r^j_s)\right\}_{f_i} \tag{12}$$

with $|\tilde{P}_{m\mu}(f_i)| = \sqrt{W_{m\mu}(f_i)}$, $\phi^k_{m\mu} = \mathrm{random}[0, 2\pi]$, and $|q^{jk}|$ does not depend on k.

Note that $W_{m\mu}$ dimension is in $\mathrm{Pa}^2/\mathrm{Hz}$, whereas $\tilde{P}_{m\mu}$ dimension is in $\mathrm{Pa}/\sqrt{\mathrm{Hz}}$. A random phase, $\phi^k_{m\mu}$, is used in order to satisfy the non-coherent mode assumption. Thus, generated sampled PSD, $\tilde{S}(f)$, should be estimated by averaging over a set of N_k realizations:

$$\tilde{S}(f, r) = \frac{1}{N_k}\sum_{k=1}^{N_k}\left\{\left(\sum_{m,\mu}\tilde{P}^k_{m\mu}(f)C_{m\mu}(r)\right)\left(\sum_{m,\mu}\tilde{P}^k_{m\mu}(f)C_{m\mu}(r)\right)^*\right\} \tag{13a}$$

In Eq. (13a), (*) denotes the complex conjugate. For uncorrelated modes, Eq. (13a) simplifies to

$$\tilde{S}(f,r) \approx \frac{1}{N_k}\sum_{k=1}^{N_k}\left\{\sum_{m,\mu}|\tilde{P}^k_{m\mu}(f)|^2 C^2_{m\mu}(r)\right\} = \sum_{m,\mu} W_{m,\mu}(f) C^2_{m\mu}(r) \tag{13b}$$

Practically (see Section 3.3), statistical errors become almost negligible when $N_k \geqslant 10$. The implementation of this source-term in a time-domain CAA code (like *sAbrinA*) should lead to a large saving in CPU time and data storage (compared to unpractical time-domain approach based on "physical" turbulent sources), so that the simulation of turbofan broadband noise propagation in a realistic aero-engine (including non-uniform flow effects) could be numerically investigated.

3. Validation cases

3.1. Uniform mean flow and shear mean flow simulations in semi-infinite annular duct

The validation case proposed is relative to a simplified turbofan exhaust provided by Qinetiq [19], and also studied by Zhang [4]. Axial section view of geometry and typical mean flow are shown in Fig. 8, the bypass-duct region of interest being pointed by a circle. A fully annular geometry is used for the present validation purpose.

Annular duct outer radius is $R = 1.46$ m, and hub-to-tip ratio is $h = 0.57$. The mean flow is deduced from a RANS solution provided by Qinetiq (Fig. 9). Radial profile of the mean axial velocity in the exhaust plane has been duplicated in the axial direction to simulate a parallel shear flow. The figure reveals a non-negligible boundary layer (about 7 percent of the duct height). Both uniform and shear flow cases are studied. Uniform mean flow is simply computed by a radial averaging, leading to a Mach number $M = 0.41$. Acoustic frequency is $f = 1450$ Hz and angular mode is $m = 13$. In these conditions, five radial modes ($\mu = 1$–5) are cut on.

Inputs to *Exfan* code are the modal amplitudes, i.e., $p_{m\mu}$ in Eq. (1), expected to be issued from the CFD unsteady data post-processing. They are arbitrarily imposed here for validation purpose. *ExFan* outputs are then entered as a source-term in *sAbrinA*. The 3D and axi-section views of the grid used for these simulations are presented in Fig. 10. Equivalent sources are injected at $z = 0$ (source-block domain), and reliable downstream propagation domain extends from 0 to 2 m. The regular grid has 30 and 170 cells in the radial and angular directions, respectively. There are axially 20 points per wavelength in the source-block domain to ensure some regularity in the three directions. Away from the source domain, the axial grid spacing is slightly increased up to the usual limit of 10 points per wavelength. Seven stretched cells are added upstream and downstream to guaranty NRBC by simply enhancing the numerical dissipation, since currently available 1D-Thompson NRBC are known to be ineffective in the presence of helicoidal waves.

First of all, the inputs of the computations need to be defined. To do that, elementary solutions of the convected Helmholtz equation are calculated and compared to the parallel shear flow solutions obtained by solving the Pridmore–Brown (P–B) equation, that is a homogeneous form of Lilley equation (i.e. no source

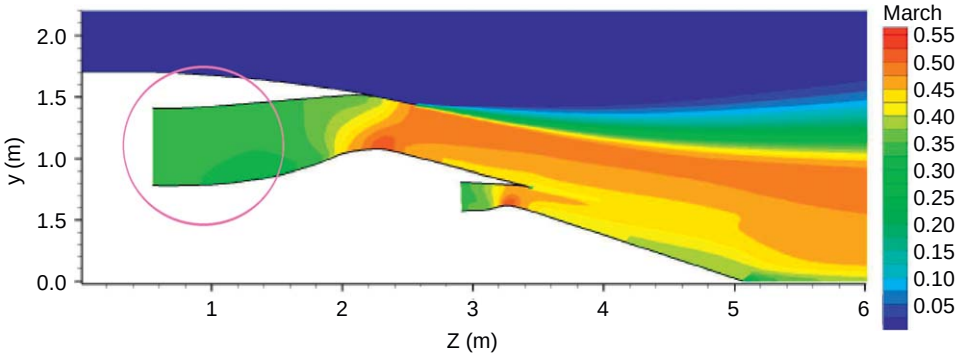

Fig. 8. Simplified turbofan ejection (Qinetiq).

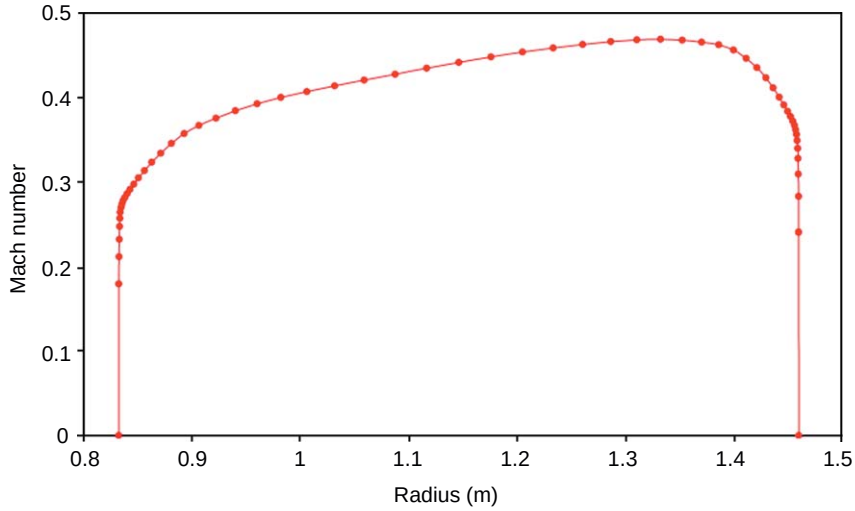

Fig. 9. Parallel shear flow (RANS) in the annular bypass duct.

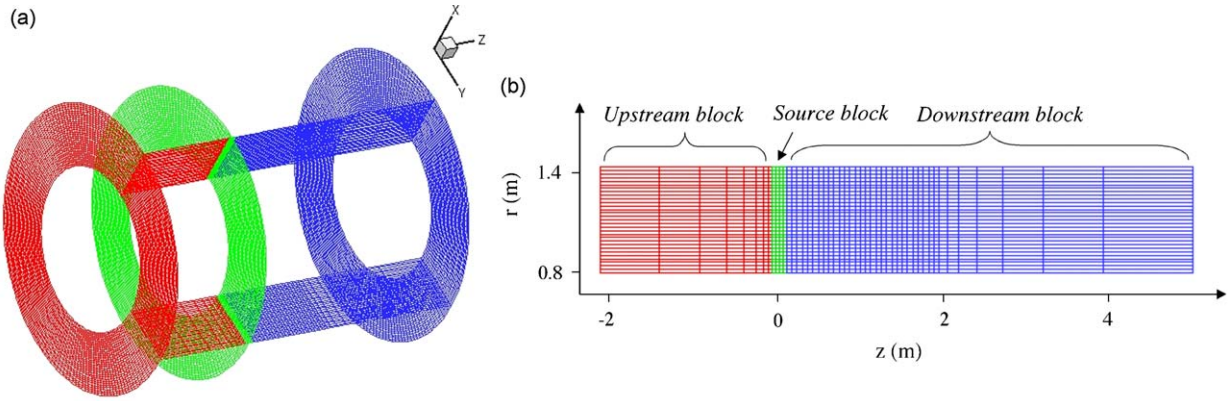

Fig. 10. CAA grid used for numerical validations (*sAbrinA*): (a) 3D view; (b) axi-section view.

terms), and by considering a modal decomposition as in [20,21]. The aim of this exercise is to show how a superposition of modes associated with a parallel shear flow can be reasonably well approximated by Fourier–Bessel modes (solutions in a uniform flow). Similarly as in Section 2.1, P–B solution can be written in terms of radial and axial (outgoing) modes:

$$p_m(r,z) = \sum_{\mu=1}^{\mu_{\max}} a_{m\mu}\chi_{m\mu}(r)\,\mathrm{e}^{-\mathrm{i}\gamma_{m\mu}z} \tag{14}$$

$\chi_{m\mu}$, $a_{m\mu}$, and $\gamma_{m\mu}$ denote the eigenfunctions, modal amplitudes, and axial wave numbers, respectively. As is done in [20], $\chi_{m\mu}$ and $\gamma_{m\mu}$ are numerically obtained using a Runge–Kutta algorithm coupled with a Newton method. Setting $p_{m\mu} = 1$ in Eq. (1), and $a_{m\mu} = 1$ in Eq. (14), the computed elementary profiles are shown in Fig. 11b, and compared to the standard Helmholtz solution (Fig. 11a). These comparisons show that the shear effects in the present case significantly modify only the lowest modes (first and second radial order), whereas the higher modes are almost unchanged. This is in accordance with Shankar's results [22]. The corresponding axial wave numbers compared in Fig. 12 are found to be close to each other too. Hence, pressure profile at the interface is adjusted to fit the P–B solution of Eq. (14), by computing the suitable modal coefficients $p_{m\mu}$. Following Shankar's approach [22], this is achieved by solving a matrix system (which is trivial when imposing

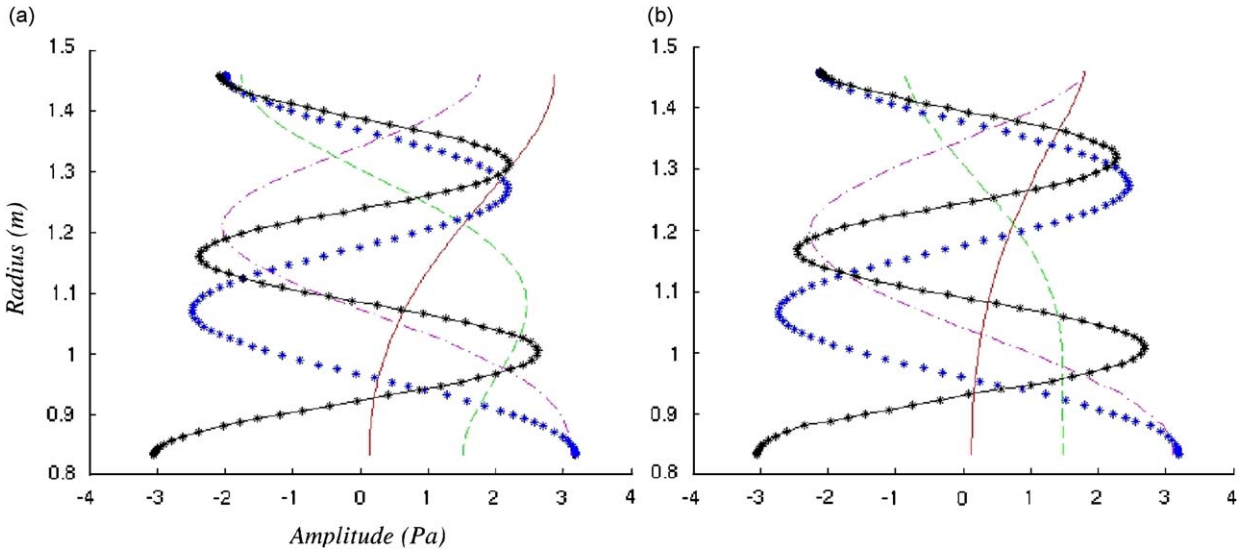

Fig. 11. Elementary pressure profiles (in Pa) relative to the five cut-on radial modes in a uniform mean flow and parallel shear flow: (a) convected Helmholtz solution; (b) Pridmore–Brown solution.

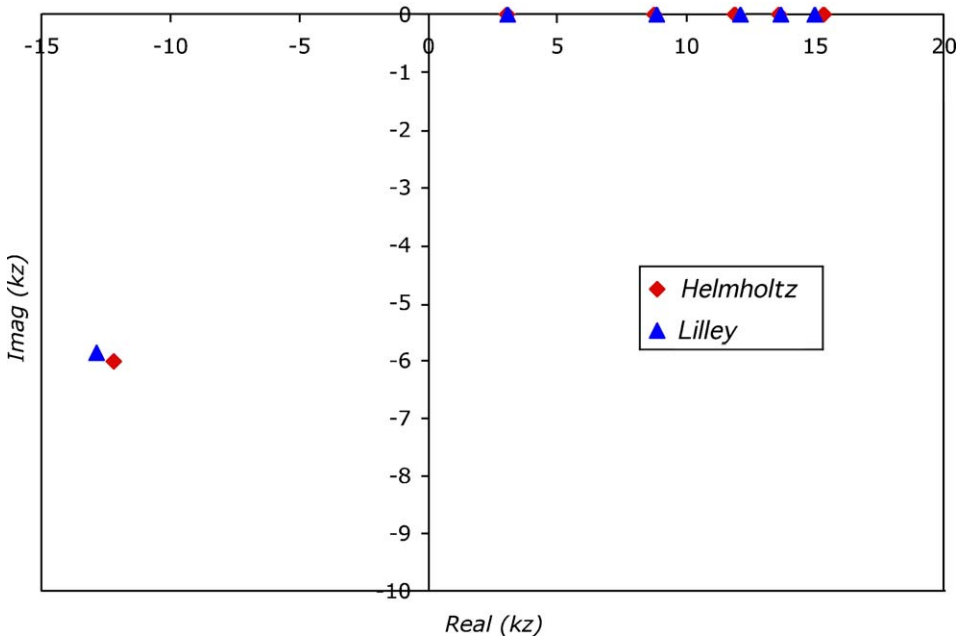

Fig. 12. Axial downstream wave numbers ($f = 1450$ Hz; $m = 13$; $\mu = 1$–6).

the values of the modal amplitudes $a_{m\mu}$ as is done here) that writes

$$\sum_{\mu=1}^{6} a_{13\mu}\chi_{13\mu}(r) = \sum_{\mu=1}^{6} p_{13\mu}C_{13\mu}(r) \tag{15}$$

Note that the first cut-off radial mode ($\mu = 6$) is also included in the prescribed field which makes this exercise well suited to practical applications. Pressure mode coefficients verifying Eq. (15), with $a_{13\mu} = 1$, are found to

be equal to

$$p_{13,1} = 0.608, \quad p_{13,2} = 0.308, \quad p_{13,3} = 1.157,$$
$$p_{13,4} = 1.15, \quad p_{13,5} = 0.767, \quad p_{13,6} = 0.995$$

The resulting pressure profiles (calculated over six modes including the first cut-off radial mode) are compared in Fig. 13 showing a quite good agreement between the two solutions.

Now all the necessary data are available to run the simulations. First validation aims at checking the ability of *ExFan* module. Calculation conditions are those described above when considering a uniform mean flow with Mach number $M = 0.41$. Prescribed modal pressure field given by Eq. (1) is plotted in Fig. 14a and compared to field generated by equivalent sources (computed by *ExFan*), and plotted in Fig. 14b. The calculation domain has been extended up to ± 4 m in the axial direction. Acoustic pressure field is characterized by complex interference patterns (due to the superposition of axial waves) with significant upstream/downstream convective effects that are perfectly predicted by the equivalent source computation, in terms of phase and amplitude. This validates the *ExFan* outputs to be used for CAA.

The next validation step concerns the source implementation in the code *sAbrinA*, as detailed in Section 2.4. Note that complementary validations have been recently published [5]. The acoustic modes considered in Fig. 14 are entered in *sAbrinA*, in a uniform mean flow, and the analytical solution of Fig. 14 (limited to the computation domain, i.e. axial range [0–2 m]) is compared to the numerical predictions using the source-based

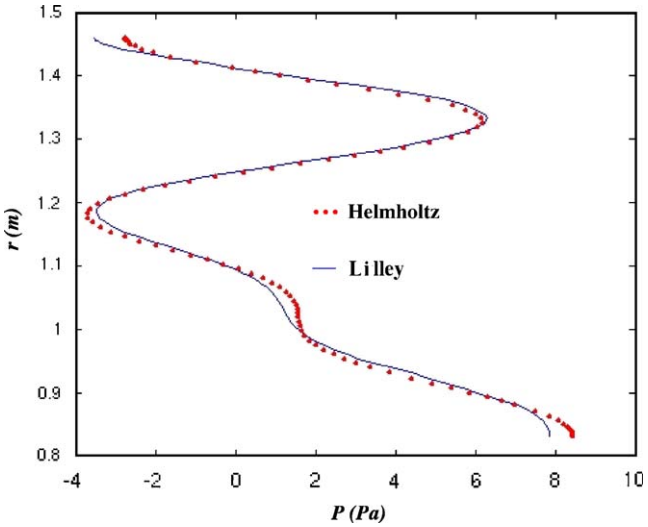

Fig. 13. Radial profiles at exhaust section ($f = 1450$ Hz; $m = 13$; $\mu = 1$–6).

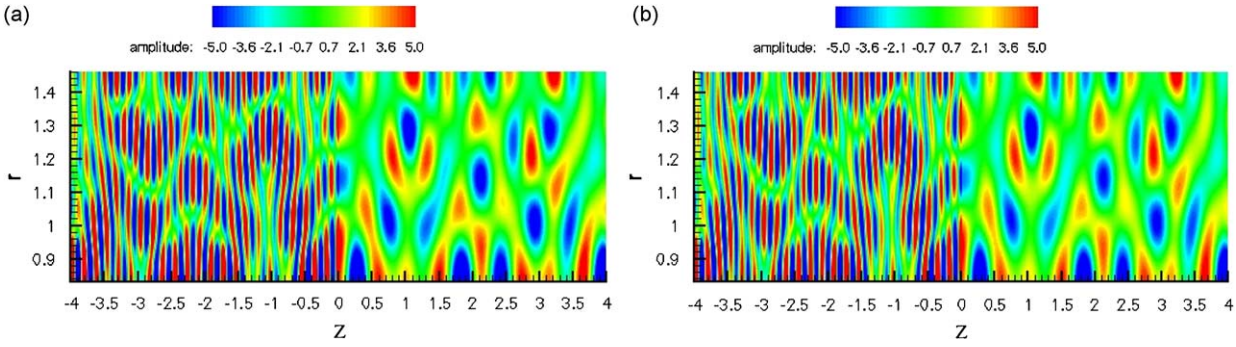

Fig. 14. Comparison between prescribed (a) and re-generated (b) instantaneous pressure fields (Pa) in a uniform mean flow.

and BC-based versions of the solver. The 2D pressure snapshots in the axial section of the duct are presented in Fig. 15, showing a very good agreement between the three solutions. In order to highlight any differences, the three solutions relative to the pressure profile along the axis are compared for two radial positions, at the hub (Fig. 16) and at the outer wall (Fig. 17). Whatever the injection process adopted (equivalent source-term or inflow BC), the numerical predictions fit fairly well the theory, even if the accuracy seems to be better with the conventional BC approach. This may be attributed to the fact that a larger number of time iterations was used for the BC-based computations with a special care to the convergence of the solution (checking the rms values), compared to the previously performed source-based computations (for which periodicity might not be fully achieved). Moreover, periodicity conditions in the azimuthal direction (recently implemented in *sAbrinA*) have been used for the BC-based computations, whereas source-based computations are fully 3D. Anyway, capability of both versions of the code are clearly demonstrated in the case of a semi-infinite duct and in the presence of a uniform mean flow.

To go further in the validations relative to the equivalent source approach, the non-uniform flow case is considered now. The parallel shear flow deduced from RANS is imposed within the source and downstream blocks, whereas uniform flow conditions are used in the upstream stretched region. The 2D pressure snapshots in the axial section of the duct are presented in Fig. 18. As expected, the pressure profile at the vicinity of the source plane ($z = 0$) is roughly unchanged compared to Fig. 15. Although the mean flow is assumed to be uniform in the equivalent source process, shear effects with respect to the downstream propagation (found to be low here) are fairly well assessed by the Euler calculation, as shows the agreement of interference patterns from P–B (Fig. 18a) and *sAbrinA* (Fig. 18b) solutions. Snapshots of numerical and semi-analytical pressure profiles along the axis are also compared in Fig. 19, at the hub (left) and at the outer wall (right). Despite of slight differences in the vicinity of the downstream boundary (probably due to non-fully converged solution),

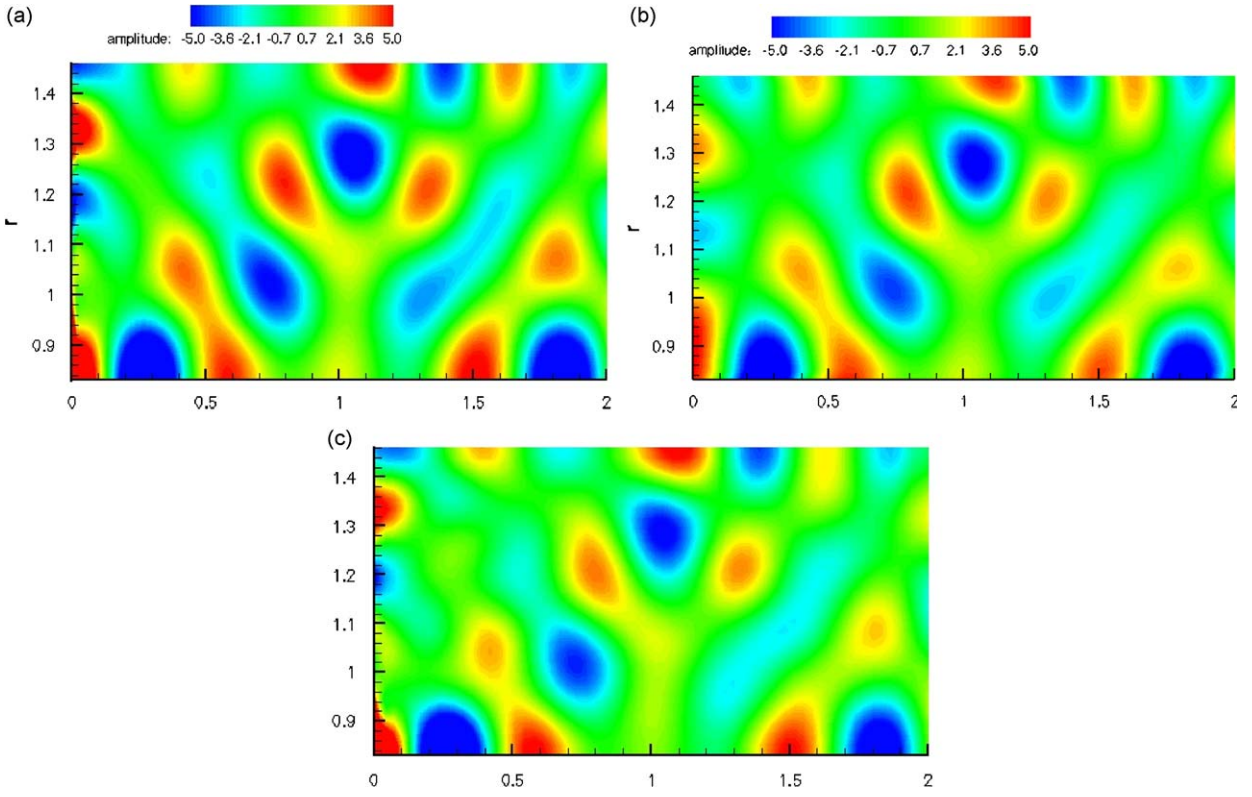

Fig. 15. Downstream propagation in a uniform mean flow ($f = 1450$ Hz, $m = 13$, $\mu = 1$–6): comparison of pressure snapshots (Pa) obtained from theory (a), *sAbrinA_BC* (b), and *sAbrinA_sources* (c).

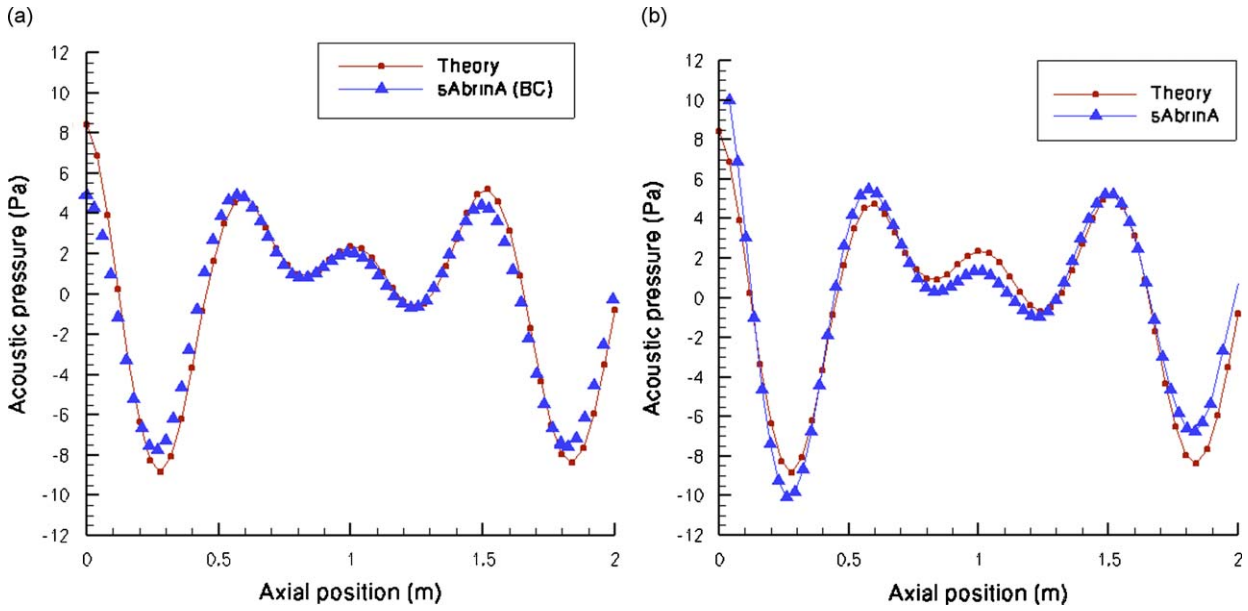

Fig. 16. Comparisons of axial profiles at hub using BC (a) or source-term (b) approach.

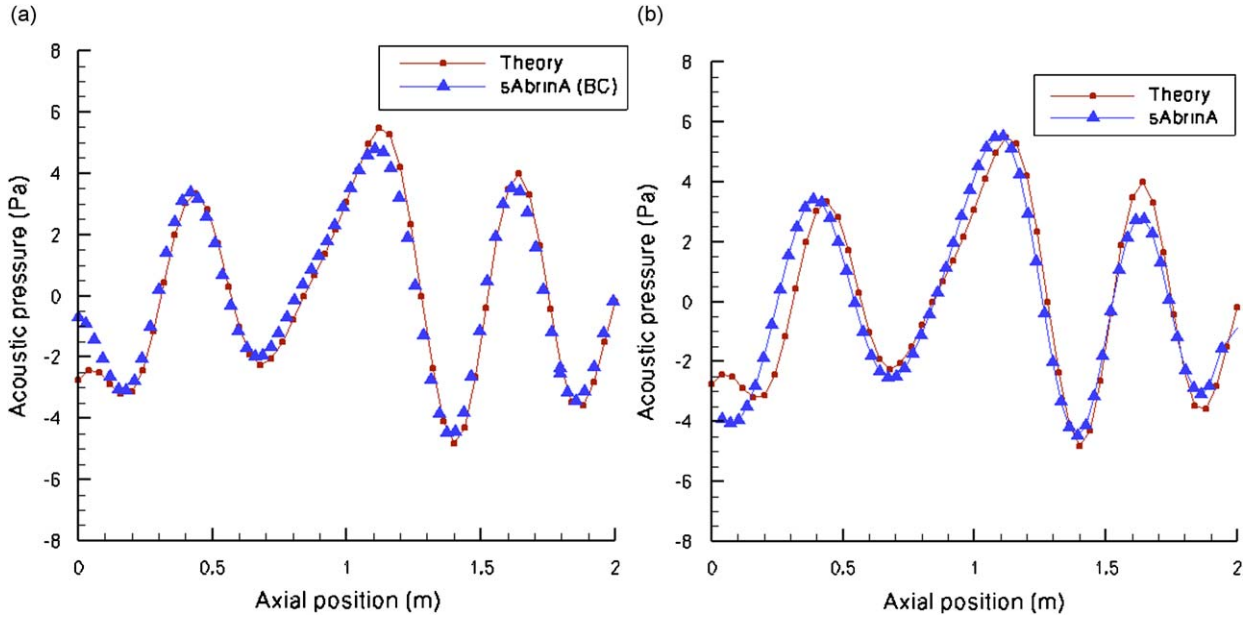

Fig. 17. Comparisons of axial profiles at outer wall using BC (a) or source-term (b) approach.

sAbrinA and P–B solutions are in a good agreement, which tends to validate the ability of the present model in the case of a parallel shear flow.

Next section is devoted to simulations of standing waves due to acoustic reflections at duct end (finite duct case), using source-based and BC-based approaches.

3.2. *Standing wave simulations in finite annular duct*

The same geometry is used here to check the ability of the equivalent source model to simulate outgoing and incoming mode propagation in the presence of a high standing wave ratio. Numerical solution obtained using

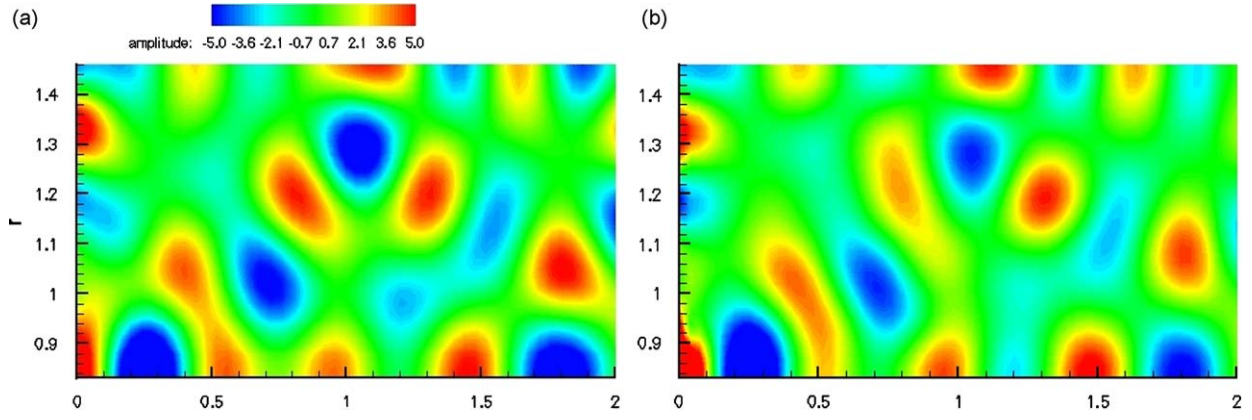

Fig. 18. Comparison between semi-analytical (a) and numerical (b) pressure snapshots (Pa), solutions of modal propagation in a parallel shear flow ($f = 1450$ Hz, $m = 13$, $\mu = 1$–6).

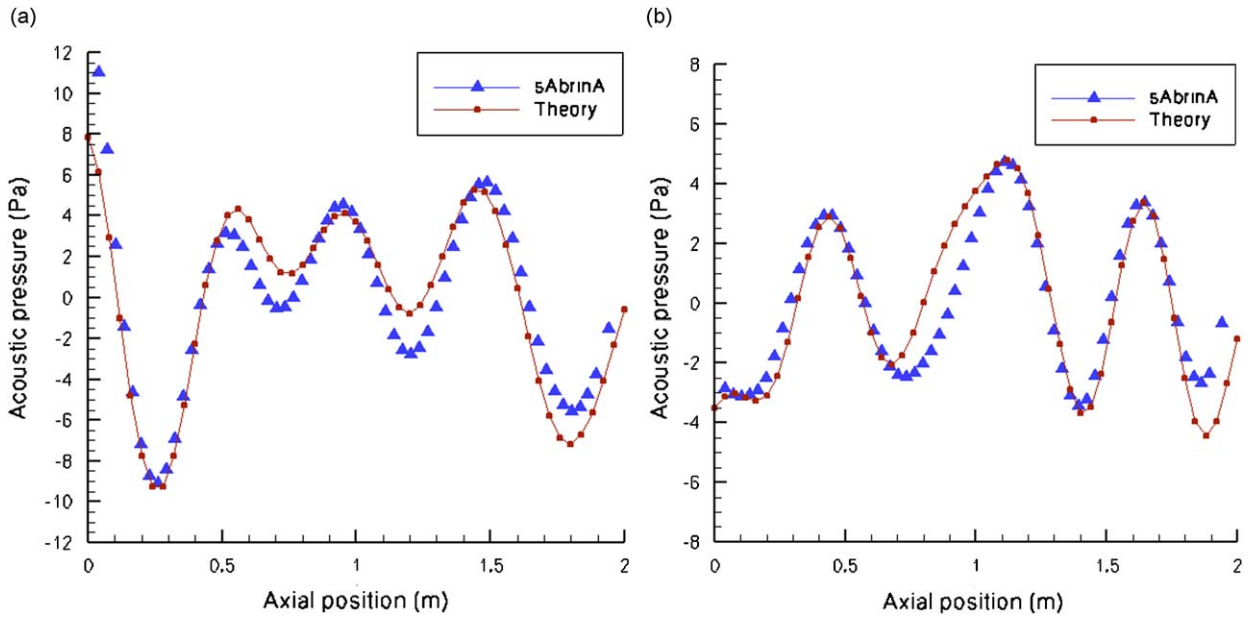

Fig. 19. Comparisons of parallel shear flow solutions at hub (a) and at outer wall (b).

an inflow BC is also investigated. The benchmark is sketched in Fig. 20. For convenience the downstream domain is limited to 1 m, and an infinite impedance ($Z_L = \infty$) is imposed at the duct end ($z = L = 1$ m). In this way, a total reflection is expected at the exit, responsible for full standing waves (standing wave ratio equal to 1) inside the duct. For simplicity, the fluid is set at rest, and we focus on single mode (13,1) at two particular frequencies: (a) $f = 650$ Hz ($\lambda_{13,1} = L$); (b) $f = 697.5$ Hz ($5/4\lambda_{13,1} = L$).

Outgoing waves with modal amplitude equal to unity and propagating in the downstream direction ($z > 0$) can be expressed as

$$P^{+}(z, r, t) = A_{13,1} C_{13,1}(r)\, \mathrm{e}^{\mathrm{i}(\omega t - k^{+}_{13,1} z)}, \quad A_{13,1} = 1 \tag{16}$$

The total pressure wave (rms value) then writes

$$P^{\mathrm{tot}}_{\mathrm{RMS}}(z, r) = C_{13,1}(r)[1 + \cos\{(k^{+}_{13,1} + k^{-}_{13,1})(z - L)\}]^{1/2} \tag{17}$$

The fluid at rest condition leads to $k^{+}_{13,1} = k^{-}_{13,1}$, so that for the two frequencies considered, the total pressure magnitude, $P^{\mathrm{tot}}_{\mathrm{mag}}$, at $z = 0$ and $z = L$, writes, respectively,

$$P^{\mathrm{tot}}_{\mathrm{mag}}(0,r) = 2P^{+}_{\mathrm{mag}}(r), \quad P^{\mathrm{tot}}_{\mathrm{mag}}(L,r) = 2P^{+}_{\mathrm{mag}}(r) \tag{18a}$$

$$P^{\mathrm{tot}}_{\mathrm{mag}}(0,r) = 0, \quad P^{\mathrm{tot}}_{\mathrm{mag}}(L,r) = 2P^{+}_{\mathrm{mag}}(r) \tag{18b}$$

These two cases are quite relevant for a benchmark, because the source plane (i.e., BC plane for the conventional inflow BC) is exactly located at a pressure anti-node (case a) or at a pressure node (case b). Comparisons between analytical and numerical predictions of the total pressure (modulus) are presented in Figs. 21 and 22, for cases (a) and (b), respectively. In these figures, the two versions of *sAbrinA*, i.e., with inflow BC (*sAbrinA_BC*) and with equivalent-source (*sAbrinA_sources*), are benchmarked. The analytical

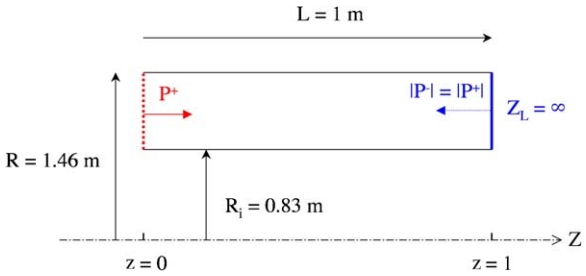

Fig. 20. Benchmark proposed for standing-wave simulations.

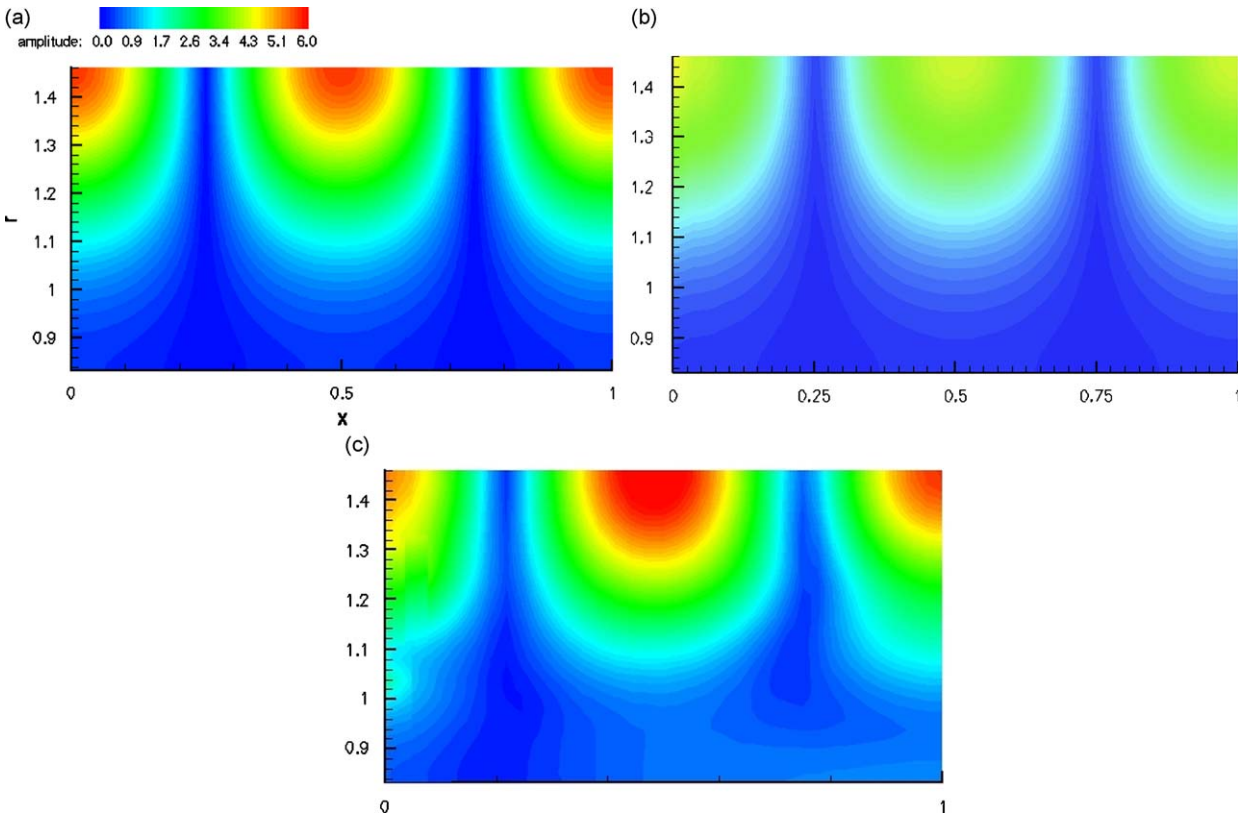

Fig. 21. Comparison between analytical (a), *sAbrinA_BC* (b), and *sAbrinA_sources* (c) solutions in a finite annular duct with total reflexion at duct end; $f = 650$ Hz.

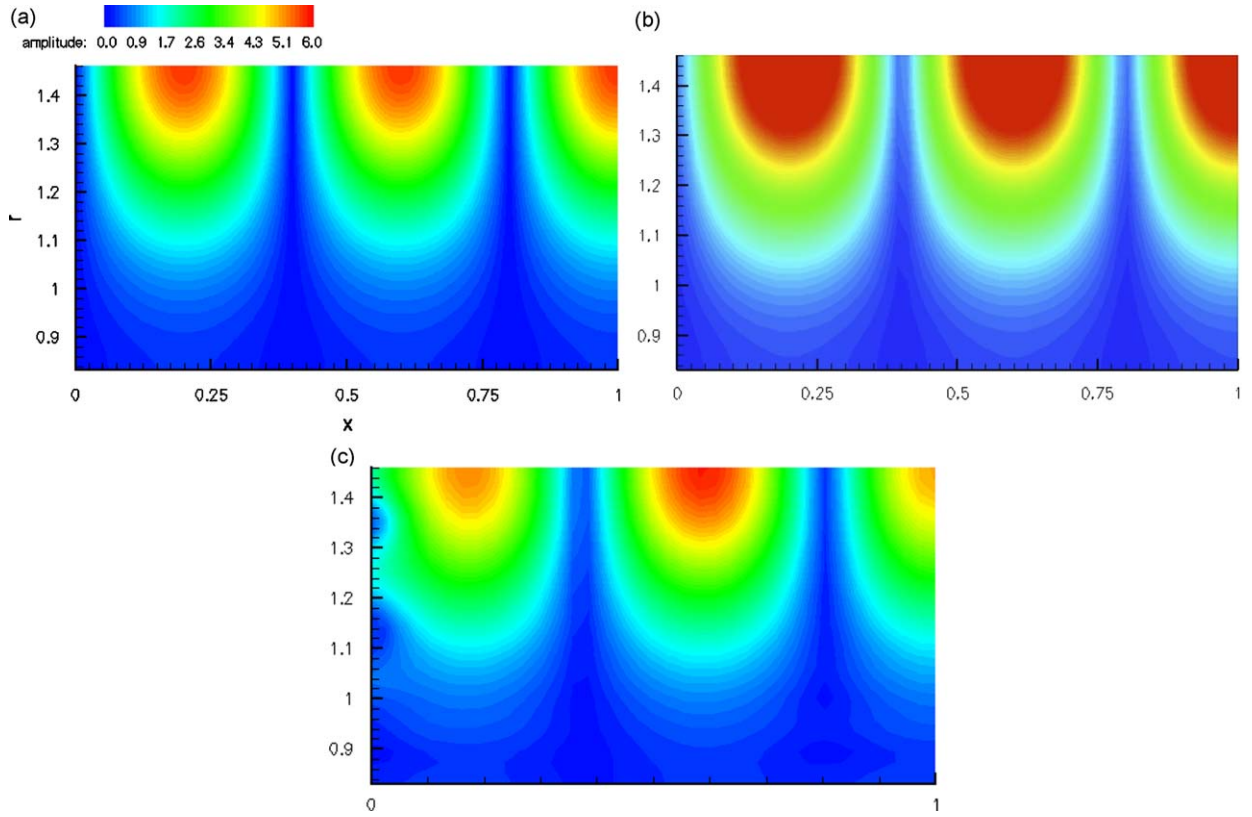

Fig. 22. Comparison between analytical (a), *sAbrinA_BC* (b), and *sAbrinA_sources* (c) solutions in a finite annular duct with total reflexion at duct end; $f = 697.5$ Hz.

solutions highlight the expected results given by Eq. (18a) and (18b). The numerical simulations are in good agreement in terms of nodes and anti-nodes location, but although *sAbrinA_BC* solution provides more regular wave lobes compared to *sAbrinA_sources*, it reveals an under-estimation (Fig. 21) or over-estimation (Fig. 22) of the pressure magnitude. This point is emphasized in Fig. 23 showing a comparison of standing wave profiles on the outer wall. Although the shape of the standing wave profiles computed by *sAbrinA_BC* fits fairly well the theory, a tuning factor (amplification or attenuation) around 1.4 with respect to the outgoing mode magnitude should be applied to fit the theoretical magnitude. This would lead, in the critical case of a quasi-total reflection at duct exit, to a noticeable uncertainty of ± 3 dB on the radiated noise level. This modulation factor between $P^{\mathrm{tot}}_{\mathrm{mag}}$ and P^{+}_{mag} is a consequence of the numerical reflections occurring at the inflow BC, due to the fact that, for each iteration time, P^{-} is set to zero for all the upstream virtual cells adjacent to the plane $z = 0$ (as explained in Section 2.3). On the other hand, despite of a slight oscillation in the wave lobes, numerical simulations with equivalent sources provide a pressure magnitude very close to the theory.

These numerical results relative to an academic (but non-trivial) case clearly demonstrate the ability of present equivalent-source approach to manage outgoing/incoming waves.

3.3. Broadband noise simulations

Let us consider the same exhaust configuration and the turbulent sources due to rotor wake interaction with the outlet guide vanes [18]. For validation purpose, prescribed turbulent sources are simply generated here by using random dipoles with arbitrary amplitude distributed along the radius, giving rise to the PSD shown in Fig. 24. The PSD is calculated using Eqs. (13a) and (13b), that is to say with (curve with crosses) and without (curve with dots) coherent mode assumption. The frequency range is limited to 5 kHz, and with a

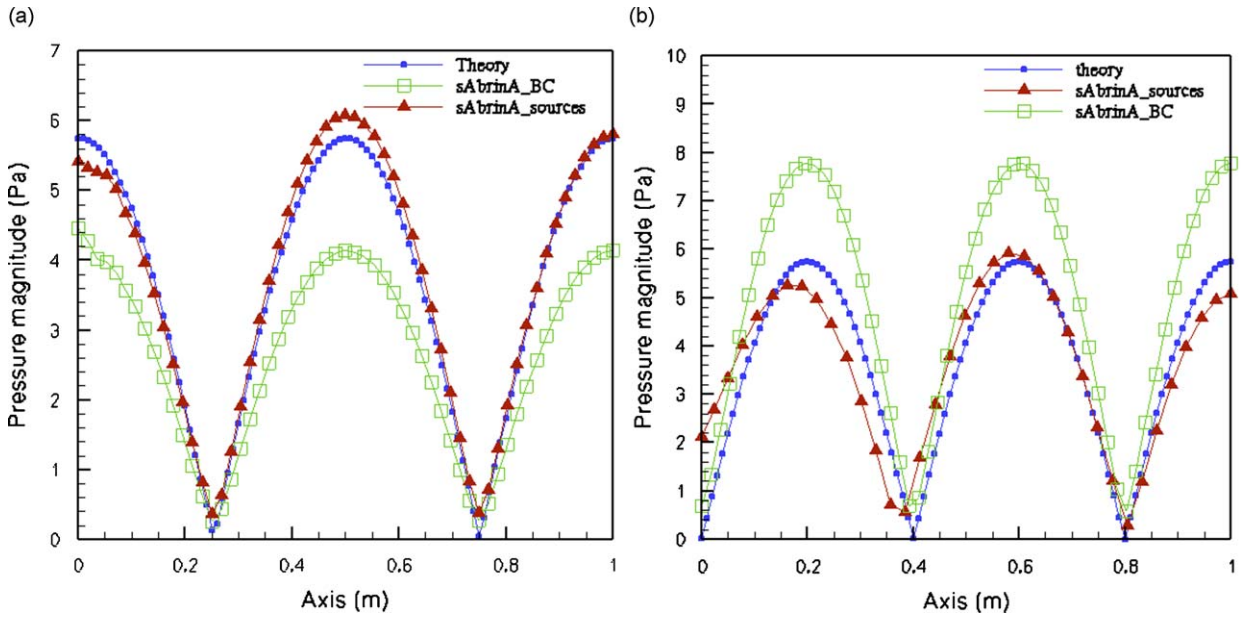

Fig. 23. Comparison between analytical and numerical standing-wave magnitude in a finite annular duct with total reflexion at duct end: (a) $f = 650$ Hz; (b) $f = 697.5$ Hz.

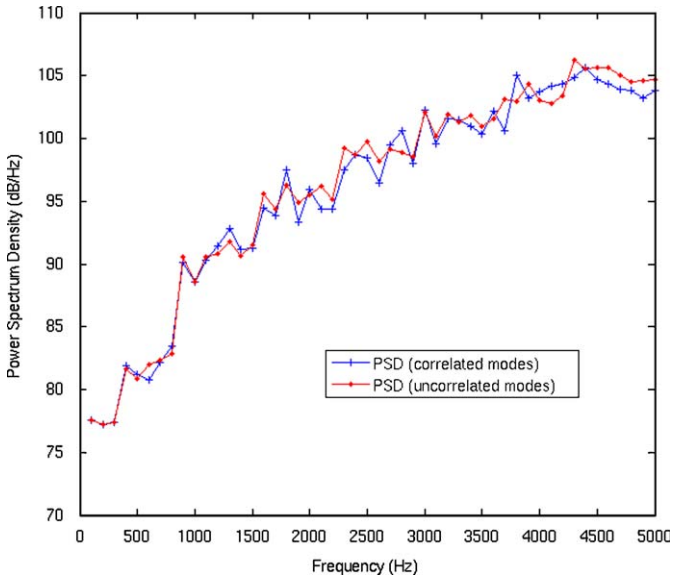

Fig. 24. Comparison of predicted PSD using correlated and uncorrelated mode assumption.

frequency-mode spectrum (see Fig. 6) characterized by maximum angular and radial cut-on mode orders, respectively, equal to $m_{\max} = 140$ and $\mu_{\max} = 22$. The frequency resolution is set equal to $\Delta f = 100$ Hz, and the statistical averaging is performed by choosing $N_k = 50$. The two PSD are found to be quite similar, which means that the modes can be assumed to be uncorrelated as is usually done for broadband noise. Then, the PSD is generated using the *ExFan* routine, by applying Eq. (12) for each frequency, and considering again the uncorrelated mode assumption as in Eq. (13b). This aims at checking the accuracy of the inverse method procedure generalized to broadband noise. Comparison of both predictions is shown in Fig. 25, showing that the regenerated PSD (star symbols) perfectly matches the initial PSD.

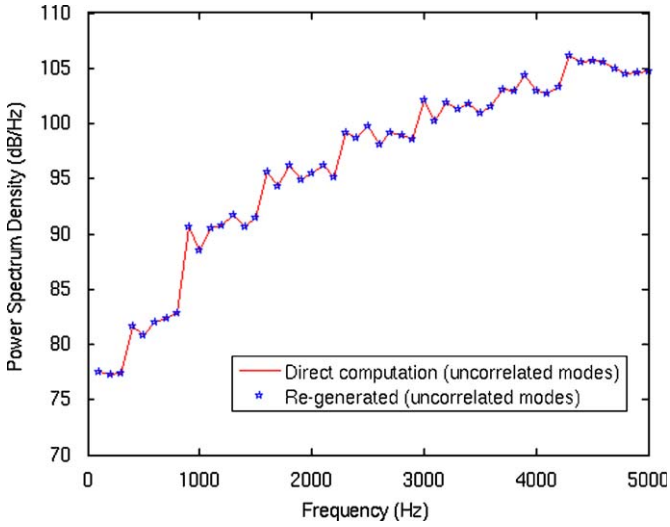

Fig. 25. Comparison between turbulent-source PSD and regenerated PSD assuming uncorrelated harmonic modes.

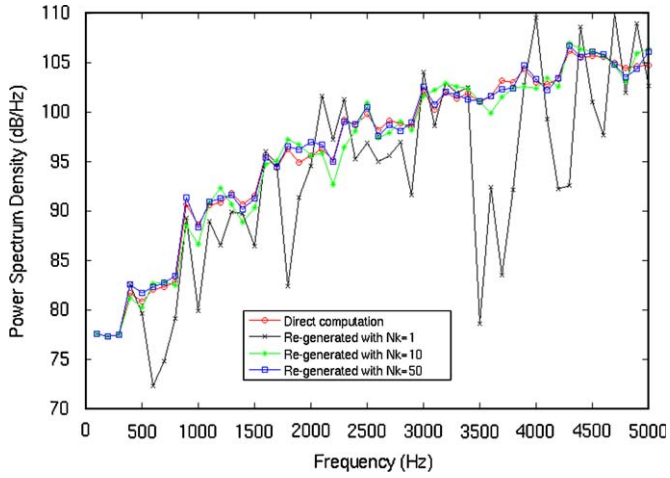

Fig. 26. Comparisons between turbulent-source PSD (direct computation) and regenerated PSD obtained using correlated harmonic modes with random phase.

Finally, since multi-mode propagation with *sAbrinA* would be inevitably achieved in a coherent way, initial PSD is re-generated by taking into account the cross-correlation terms in Eq. (13a), and by making it decrease as more as possible thanks to the averaging. In Fig. 26, initial PSD (curve with circles) is compared to the equivalent PSD, obtained by setting $N_k = 1$ (curve with crosses), $N_k = 10$ (curve with stars), and $N_k = 50$ (curve with squares). As mentioned in Section 2.5, convergence is reasonably achieved when $N_k \geqslant 10$.

Practically, numerical simulations with *sAbrinA* could be realized by launching N_k (about 10) runs, and by estimating the PSD with an averaging over each batch.

4. Conclusions and perspectives

A matching model aimed at coupling fan interaction noise generation (CFD issue) to in-duct acoustic propagation (CAA issue) has been presented and validated in this paper. Disturbance field at the interface is classically expanded over incoming/outgoing acoustic modes. Although the local assumptions considered

(straight annular geometry and uniform mean flow) are more restrictive compared to Rienstra slowly varying modes strategy, the originality of the process is that the outgoing modes are injected by means of equivalent sources in the CAA, instead of being implemented as a BC. In this way, standing waves due to reflections at open duct ends (or due to the presence of a liner) expect to be accurately captured. The use of present model for generating equivalent turbulent sources responsible for broadband noise in ducted fans has been also tackled.

A benchmark relative to a turbofan bypass duct has been studied. Simulation of representative propagating modes in a uniform mean flow and a shear mean flow (provided by RANS) has been performed by implementing the equivalent sources in a CAA Euler code, *sAbrinA*. Numerical simulations based on two options in *sAbrinA* (usual inflow BC and equivalent-source term) are found to be very close to the analytical solution, and thus seem to be quite reliable. An academic but relevant benchmark, based on the same configuration, has also been proposed to check the accuracy of mode propagation in the presence of standing waves (in the case of a total reflection at duct exit). Numerical simulations have been validated by comparisons with analytical solutions, showing the advantage of the source approach that provides very accurate results, whereas the use of inflow BC may give rise to a noise level uncertainty of ± 3 dB, caused by artificial numerical reflections occurring in the BC plane. Finally, some promising validations regarding the extension of the equivalent source model to generate turbulent-like harmonic sources with equivalent PSD have been also proposed.

As a first industrial application, aeroacoustic analyses of a contra-rotating fan using RANS (*elsA*) and Euler (*sAbrinA*) ONERA codes, coupled by means of the present model have been recently performed [17], in the framework of European project VITAL. A challenging perspective is to apply the equivalent-source model to compute realistic broadband noise propagation in ducted fans, by coupling a LES-based calculation with *sAbrinA*.

References

[1] E. Envia, A.G. Wilson, D.L. Huff, Fan noise: a challenge to CAA, *International Journal of Computational Fluid Dynamics* 18 (6) (2004) 471–480.
[2] V. Ahuja, Y. Ozyoruk, L.N. Long, Computational simulations of fore and aft radiation from ducted fans, AIAA 2000-1943, *Sixth AIAA/CEAS*, Lahaina (Hawaii), 2000.
[3] R.T. Biedron, C. Rumsey, G.G. Podboy, M.H. Dunn, Predicting the rotor–stator interaction acoustics of a ducted fan engine, *39th AIAA ASME*, Reno, USA, 2001.
[4] X. Zhang, X.X. Chen, C.L. Morfey, B.J. Tester, Computation of fan noise radiation through a realistic engine exhaust geometry with flow, AIAA 2003-3267, *Ninth AIAA/CEAS*, Hilton Head, USA, 2003.
[5] C. Polacsek, S. Burguburu, S. Redonnet, M. Terracol, Numerical simulations of fan interaction noise using a hybrid approach, *AIAA Journal* 44 (6) (2006) 1188–1196.
[6] R.P. Dougherty, A wave-splitting technique for nacelle acoustic propagation, AIAA 97-1652, *Third AIAA/CEAS Aeroacoustics Conference*, Atlanta, USA, 1997.
[7] N.C. Ovenden, S.W. Rienstra, Mode-matching strategies in slowly varying engine ducts, AIAA 2003-3139, *Ninth AIAA/CEAS*, Hilton Head, USA, 2003.
[8] A.A. Ali, O.V. Atassi, H.M. Atassi, Derivation and implementation of inflow/outflow conditions for aeroacoustic problems with swirling flows, *Seventh AIAA/CEAS*, Maastricht, The Netherlands, 2001.
[9] R.J. Astley, V. Hii, G. Gabard, Computational mode matching approach for propagation in three-dimensional ducts with flow, AIAA 2006-2528, *12th AIAA/CEAS*, Boston, USA, 2006.
[10] Y. Druon, S. Lidoine, M. Roger, Acoustic radiation modeling of engine exhaust. Comparisons between analytical and numerical methods, AIAA 2004-2990, *10th AIAA/CEAS*, Manchester, UK, 2004.
[11] X.D. Li, N. Schoenwald, J. Yan, F. Thiele, A numerical study on the acoustic radiation from a scarfed intake, AIAA 2003-3245, *ninth AIAA/CEAS*, Hilton Head, USA, 2003.
[12] S. Redonnet, E. Manoha, P. Sagaut, Numerical simulation of propagation of small perturbations interacting with flows and solid bodies, AIAA 2001-2223, *Seventh CEAS/AIAA Aeroacoustics Conference*, Maastricht, The Netherlands, 28–30 May 2001.
[13] E. Manoha, S. Redonnet, M. Terracol, R. Guénanff, *Numerical Simulation of Aerodynamic Noise*, ECCOMAS 2004, Jyväskylä, Finland, 24–28 July 2004.
[14] S.W. Rienstra, W. Eversman, Sound propagation in slowly varying lined flow ducts of arbitrary cross-section, *Journal of Fluid Mechanics* 495 (2003) 157–171.
[15] A.J. Cooper, N. Peake, Propagation of unsteady disturbances in a slowly varying duct with mean swirling flow, *Journal of Fluid Mechanics* 445 (2001) 207–234.

[16] O.V. Atassi, Propagation and stability of vorticity–entropy waves in a non-uniform flow, *Journal of Fluid Mechanics* 575 (2007) 149–176.
[17] C. Polacsek, R. Barrier, Numerical simulation of counter-rotating fan aeroacoustics, *13th AIAA/CEAS Aeroacoustics Conference*, Roma, Italy, 2007.
[18] J. Riou, S. Léwy, S. Heib, *Large Eddy Simulation for Predicting Rotor–Stator Broadband Interaction Fan Noise*, Internoise 2007, Istanbul, Turkey, August 2007.
[19] S. Redonnet, E. Manoha, O. Kenning, Numerical simulation of the downstream fan noise and jet noise of a coaxial jet with a shielding surface, AIAA 2004-2991, *10th AIAA/CEAS Aeroacoustics Conference*, Manchester, UK, 2004.
[20] K.A. Kousen, Eigenmodes of ducted flows with radially dependent axial and swirl velocity components, NASA/CR Report 1999–208881, March 1999.
[21] G. Vilenski, S. Rienstra, Acoustic modes in a ducted shear flow, AIAA 2005-3024, *11th AIAA/CEAS Aeroacoustics Conference*, Monterey, USA, 2005.
[22] P.N. Shankar, Acoustic refraction and attenuation in cylindrical and annular ducts, *Journal of Sound and Vibration* 22 (2) (1972) 233–246.